IET Radar, Sonar & Navigation

*Research Article*

IET Journals
The Institution of Engineering and Technology

# Automatic feature extraction from jet engine modulation signals based on an image processing method

ISSN 1751-8784
Received on 9th June 2014
Accepted on 23rd October 2014
doi: 10.1049/iet-rsn.2014.0281
www.ietdl.org

*Yang Woo Yong*[1,2] ✉, *Park Ji Hoon*[1], *Bae Jun Woo*[2], *Kang Sung Cheol*[2], *Myung Noh Hoon*[1]

[1]*Department of Electrical Engineering, Korea Advanced Institute of Science and Technology (KAIST), 335 Gwahangno, Yuseong-gu, Daejeon, 305-701, Republic of Korea*
[2]*Samsung Thales, Bundang-Gu, Seongnam 463-400, Republic of Korea*
✉ *E-mail: diddndyd@kaist.ac.kr*

**Abstract:** This study presents an automatic method for extracting the jet engine features from the joint time-frequency (JTF) representation of jet engine modulation (JEM) signals. First, empirical mode decomposition with adaptive low-pass filtering was employed to extract the first harmonic component of the JEM signal. Then, a smoothed pseudo Wigner–Ville distribution (SPWVD) technique was used for acquiring the refined JTF representation. After converting the SPWVD result into an image with RGB colours, the green component was extracted as a representative of the JEM component. Finally, the peaks detected from the extracted green component can represent the jet engine features. The approach proposed in this study is significant because the overall procedures for extracting the jet engine features are not manual but automatically performed based on the image processing method. Application to measured JEM signals demonstrated that the automatic feature presented in this study improved the accuracy of JEM analysis and is expected to be efficient for real-time radar non-cooperative target recognition.

## 1 Introduction

Jet engine modulation (JEM) has been widely used as a representative radar target recognition method by providing unique information on targets. JEM, induced by electromagnetic scattering from a rotating jet engine compressor, is one of the micro-Doppler phenomena that impart frequency modulation to radar signals [1–4]. For JEM analysis, various methods have been adopted to acquire useful information on jet engines, such as the rotation rate and the blade number (BN). In previous studies, time-domain methods, such as auto-correlation, have been used for estimating fundamental periodicity of JEM signals [5–7]. The spectrum in the frequency domain has been used to estimate the BN equipped in the first rotor stage [7]. In recent years, joint time-frequency analysis (JTFA) for feature extraction has been employed to complement these single-domain methods and has provided physical insight into time-dependent characteristics of JEM signals as in other cases of micro-Doppler analysis [8–16].

However, in most studies associated with JTFA of JEM signals, the jet engine information is obtained by manually estimating the signal characteristics from joint time-frequency (JTF) representation. When manual estimation is carried out by the researcher, the JEM analysis may be inaccurate in extracting the jet engine features. In addition, because of its time-consuming nature, manual estimation is inappropriate for the real-time identification between friend and foe in the battlefield.

This paper describes the automatic extraction of the jet engine features based on an image processing method. Although there are a variety of signal decomposition methods, we employ empirical mode decomposition (EMD) because of its data-driven characteristic for which there is no prior assumption on the given input signal [15]. On the assumption that the first chopping harmonic of the JEM spectrum is sufficiently discernible, EMD plays a role in extracting this spectral component. As described in [16], however, EMD is restricted to completely extracting the first harmonic component because of its attribute as a dyadic filter bank. Thus, EMD is modified by inserting an adaptive low-pass filter (LPF) whose cut-off frequency is given as the fundamental chopping frequency. To obtain a JTF representation clearly exhibiting the rotation-induced micro-Doppler, smoothed pseudo Wigner–Ville distribution (SPWVD) is applied to a desirable combination of intrinsic mode functions (IMFs) derived from the modified EMD operation. With the refined SPWVD result, we propose an image processing method for automatically extracting the jet engine features without any manual procedures. First, the SPWVD result is converted into an image consisting of RGB colours. Then, the RGB image is processed to extract the green component, which is regarded as containing the effective JEM component. Finally, the peaks detected from the extracted green component can represent the jet engine features. The approach proposed in this paper is significant because the overall procedures for extracting the jet engine features are not manual but automatically performed based on the image processing method. Therefore, the proposed method for feature extraction is expected to be applied to real-time non-cooperative target recognition (NCTR).

The rest of the paper is organised as follows: Section 2 presents the proposed method for automatic extraction of jet engine features. In Section 3, the measured JEM signals are examined to validate applicability of the proposed method. Finally, conclusions and future work are discussed in Section 4.

## 2 Method for automatic extraction of jet engine features

### 2.1 Reconstruction of JEM signals in the JTF domain before image processing

To extract jet engine information based on the image processing method, it is necessary to obtain a JTF representation of the JEM signal that clearly shows the typical characteristics of the rotation-induced micro-Doppler. However, most JEM signals commonly exhibit an obscure and irregular JTF representation because of their complicated frequency composition. Thus, the

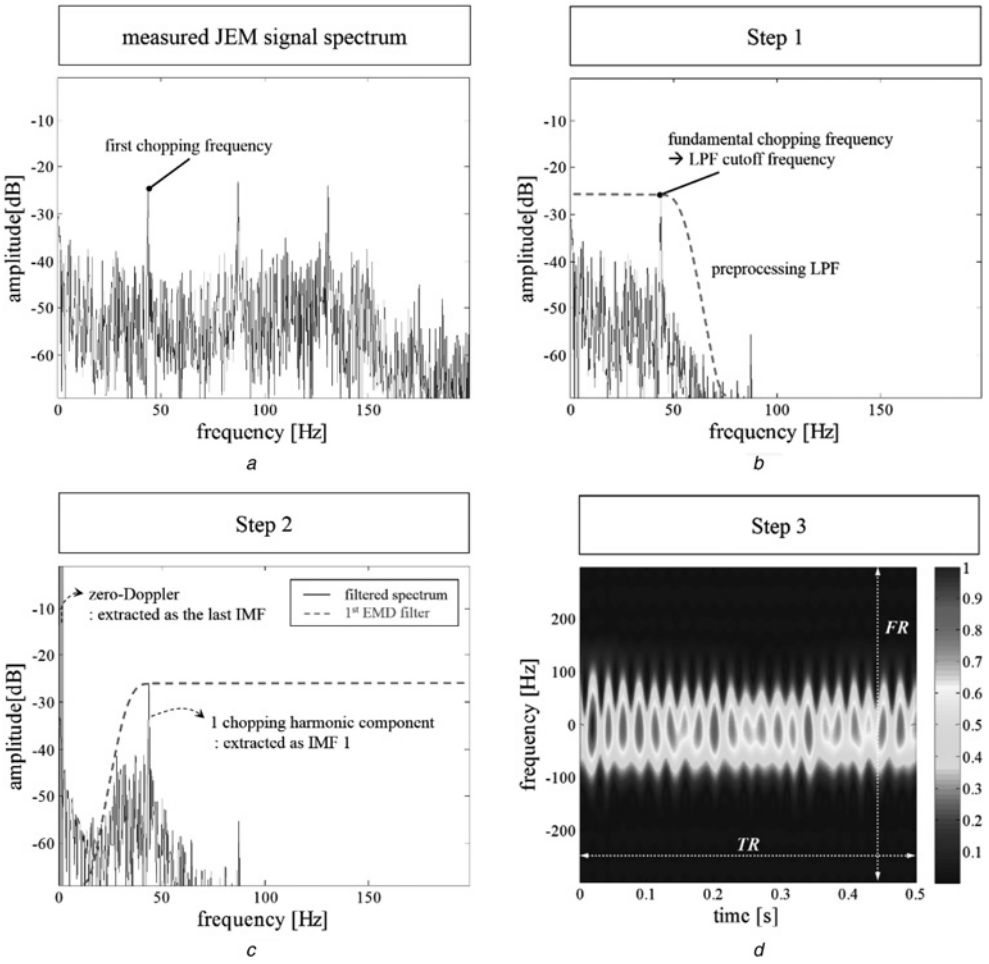


**Fig. 1** *Overall procedures for reconstructing JEM signals*

*a* Original JEM spectrum with complicated frequency components
*b* JEM spectrum after applying *a* to the LPF
*c* JEM spectrum of IMF 1 combined with the last IMF
*d* SPWVD result of the combined signal of *c*

JTF representation is refined via the following reconstruction procedures for JEM signals (also summarised in Fig. 1):

*Step 1:* Selection of the cut-off of the preprocessing LPF as the fundamental chopping frequency.
*Step 2:* Decomposition of the signal filtered by the LPF into a finite number of IMFs using EMD.
*Step 3:* Application of the SPWVD technique to the desirable combination of extracted IMFs to obtain a refined JTF representation of the JEM signal.

In Step 1, the LPF whose cut-off frequency is selected as the fundamental chopping frequency is inserted as a preprocessor of EMD to supplement its filter bank property and to completely extract the first chopping harmonic component. According to [16], the first chopping harmonic plays an important role in reconstructing the rotation-induced micro-Doppler, and the JTFA of JEM signals is carried out based on the extraction of this spectral component, which is directly related to the chopping rate, the period of a propeller blade moving to its adjacent position. Since the first harmonic component generally has larger amplitude than other JEM line spectra in many cases of measured JEM signals [15, 16], it is easy to determine the cut-off frequency of the LPF by simply searching for the first harmonic component in the JEM spectrum. Fig. 1*b* presents the resultant spectrum after applying the original JEM spectrum of Fig. 1*a* to the preprocessing LPF.

In Step 2, EMD, a data-driven decomposition method for non-linear and non-stationary signals [17–19], is applied to the signal derived from Step 1. Owing to the preprocessing filtering, the first chopping harmonic component is automatically assigned to the EMD filter number 1. Moreover, IMF 1 has the centre frequency in accordance with the cut-off frequency and contains the first chopping harmonic which denotes the effective JEM component [10, 16]. Since the EMD filter of number 1 operates as a high-pass filter, EMD combined with the LPF equivalently behaves like a band-pass filter with the centre frequency same as the fundamental chopping frequency. In addition, the last IMF with the slowest oscillatory mode corresponds to the zero-Doppler component and is also required for obtaining the well-presented JTF representation in the next step. Fig. 1*c* shows the spectrum of IMF 1 combined with the last IMF resulting from the modified EMD operation to the filtered spectrum.

In Step 3, the SPWVD technique is used for obtaining a refined JTF representation of the JEM signal with complicated frequency components. SPWVD is a representative of Cohen's class and provides a good compromise between the reduction in the cross-interference and the maintenance of sufficient time-frequency resolution [10, 20]. Note that the length of smoothing function (also referred to as the length of the windows) for SPWVD should be shorter than one cycle of the modulation frequency to produce an accurate instantaneous Doppler frequency. The resolution of the SPWVD may be restricted to visualising the weakly-modulated micro-Doppler. However, because the jet engine blade length (BL) is generally larger than the radar wavelength $\lambda$, the SPWVD is sufficient for representing the rotation-induced micro-Doppler. For real application for JEM, once the adequate length of the


*IET Radar Sonar Navig.*, 2015, Vol. 9, Iss. 7, pp. 783–789

smoothing functions is designated to visualising the micro-Doppler, the length of the smoothing functions was chosen inversely related to the modulation frequency. In this paper, SPWVD yields an approximate JTF representation of the rotation-induced micro-Doppler by applying it to the combined signal with IMF 1 and the last IMF, which denotes the first harmonic component and the zero-Doppler component, respectively. This refined JTF representation makes it easy to automatically extract useful information on the jet engine via the image processing method, which will be presented in the next section. Fig. 2 shows the SPWVD results of the measured raw JEM signal with complicated frequency components and the IMF 1 extracted from the signal, respectively. In contrast to the SPWVD results in Fig. 2, useful information can now be obtained from the well-presented JTF representation shown in Fig. 1*d*. In summary, the reconstruction process described above is expected to be applicable to obtaining the refined JTF representation of the JEM signal from which automatic feature extraction can be facilitated.

### 2.2 Proposed image processing method

With the refined JTF representation, useful information on the jet engine can be extracted automatically using the image processing method. The overall procedures are illustrated in Fig. 3 and summarised as follows:

*Step 1:* Extraction of the green component from the image composed of RGB colours converted from the JTF representation.
*Step 2:* Extraction of upper and lower contours from the green component and selection between them based on variance.
*Step 3:* Peak detection from the selected contour.
*Step 4:* Acquisition of the jet engine information using the detected peaks and the proposed equations for automatic feature extraction.

In Step 1, the SPWVD result represented in the JTF domain is converted into an image consisting of RGB colours. Note that this RGB image is an $M \times N \times 3$ array of colour pixels, and each white pixel is a triplet corresponding to the red, green, or blue component at a specific spatial location. $M$ and $N$ are the numbers of vertical and horizontal pixels in the RGB image, respectively. Fig. 4, respectively, shows the red, green and blue components extracted from the RGB image. As discussed in [15, 16], the red component corresponding to high intensity, that is, at least more than 70% of the maximum amplitude is not sufficient to represent the contour resulting from the rotation-induced micro-Doppler. Although the blue component can include the outermost contour of the micro-Doppler, this colour component also resides in a region in which no signal components exist, and thus the contour may be blurred. In contrast, the green component gives a compromise between these two components and better represents the regular contour of the JEM component as shown in Fig. 4*b*. Based on the fact that the green component can become a representative of the JEM component, we focus on this colour component of the RGB image for extracting the jet engine features. Note that this component can be extracted using the image processing toolbox in MATLAB.

In Step 2, upper and lower contours are extracted from the green component exhibited in Fig. 3*a*. Although the green component is somewhat symmetrical with respect to the horizontal axis located at the centre of vertical pixels, the shapes of two contours are slightly different from each other as observed from Fig. 3*b*. Note that the upper and lower contours originate from the signal component scattered by approaching and receding jet engine blades tips, respectively. Between them, the one with more variance is selected for the next step because the fast-varying contour enables stable extraction of peaks.

In Step 3, peak detection is applied to the selected contour as shown in Fig. 3*c* where the effective peaks are marked by small triangles. Since each peak denotes periodicity of the JEM component, it is important to effectively detect these peaks from the selected green component contour that appears to be an oscillatory curve. In the peak detection process, it is necessary to define an appropriate user-defined threshold for determining if each peak is significantly larger than other time samples around it.

In Step 4, the JEM analysis is performed and the information on the jet engine is automatically obtained by image processing. The result of peak detection includes two main parameters of the jet engine, the number and the length of the compressor blades. The BN is determined by the number of outstanding peaks of the regular waveform within the spool rate. The pixel interval between adjacent peaks denotes the time interval between outstanding peaks of the regular waveform in the JTF representation. In addition, because the full range of the time domain corresponds to the number of pixels in the horizontal axis, the BN can be found from the following mathematical equation

$$\mathrm{BN} = R\left[\frac{\mathrm{HPN}}{\mathrm{FP} \times \mathrm{TR} \times f_{\mathrm{R}}}\right] \tag{1}$$

where $R[\bullet]$ is the round-off operator, HPN is the number of pixels in the horizontal axis, FP is the most frequent pixel interval between adjacent peaks, TR is the full range of the time axis in the JTF representation and $f_{\mathrm{R}}$ is the spool rate indicating the one rotation frequency (number of revolutions per second) and can be automatically estimated using the time interval between auto-correlation function peaks without the prior information on the BN [6]. For example, TR can be estimated as 0.5 from the JTF representation in Fig. 1*d*, and FP and HPN can be found as 17 and 365 as denoted in Fig. 3*c*. $f_{\mathrm{R}}$ can be found as 1.0345 Hz using the time-domain signal or its auto-correlation. Hence, the BN can be calculated as 42 using (1).

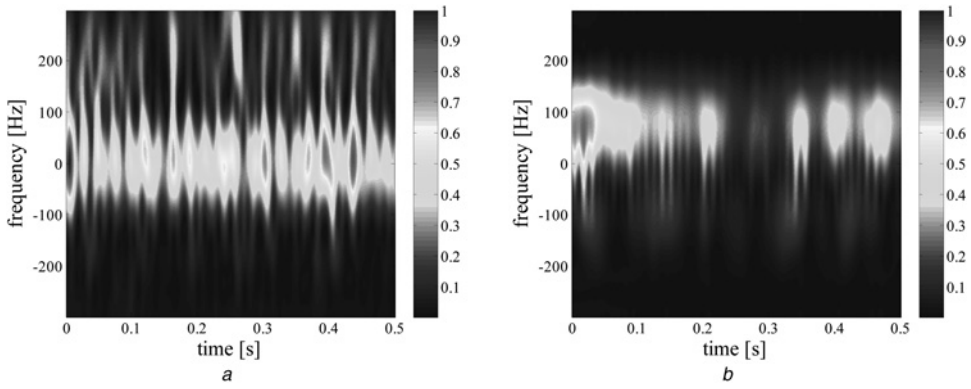


**Fig. 2** *SPWVD results of*
*a* Measured raw JEM signal and
*b* Extracted IMF 1

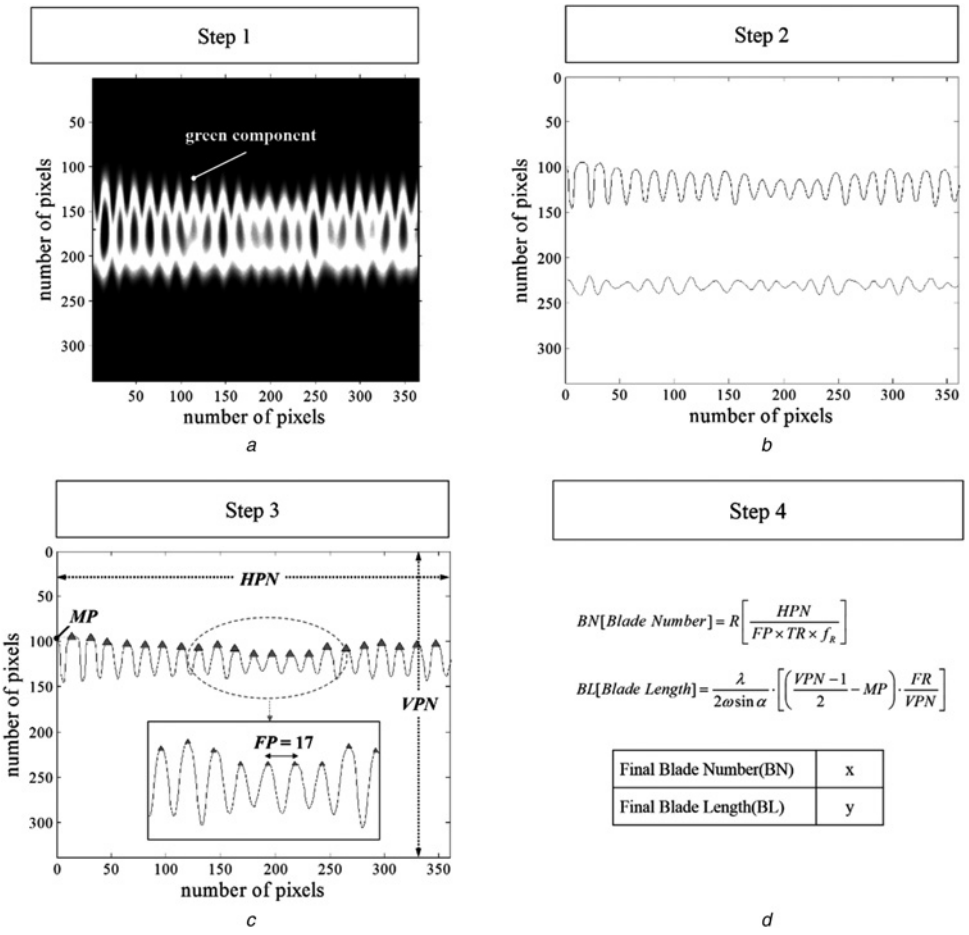


**Fig. 3** *Overall procedures of the image processing method*

*a* Green component extracted from the RGB image
*b* Upper and lower contours extracted from the green component
*c* Peak detection from the selected contour
*d* Acquisition of the jet engine information using proposed (1) and (3)

The BL can be estimated by calculating the minimum index of the vertical pixel related to the maximum Doppler-shift frequency of the JTF representation given as follows [14, 15, 21]

$$f_{\mathrm{d,max}} = \frac{2\omega L \sin\alpha}{\lambda} + C \tag{2}$$

where $f_{\mathrm{d,max}}$ is the maximum Doppler shift frequency, $\omega$ is the angular speed, $L$ is the length of blade, $\alpha$ is the angle between the direction of the rotation axis and the radar line of sight (LOS), $\lambda$ is the wave length and $C$ is the constant resonance value resulting from the cavity effect of the jet engine structure that causes the frequency offset in the JTF representation. However, because this

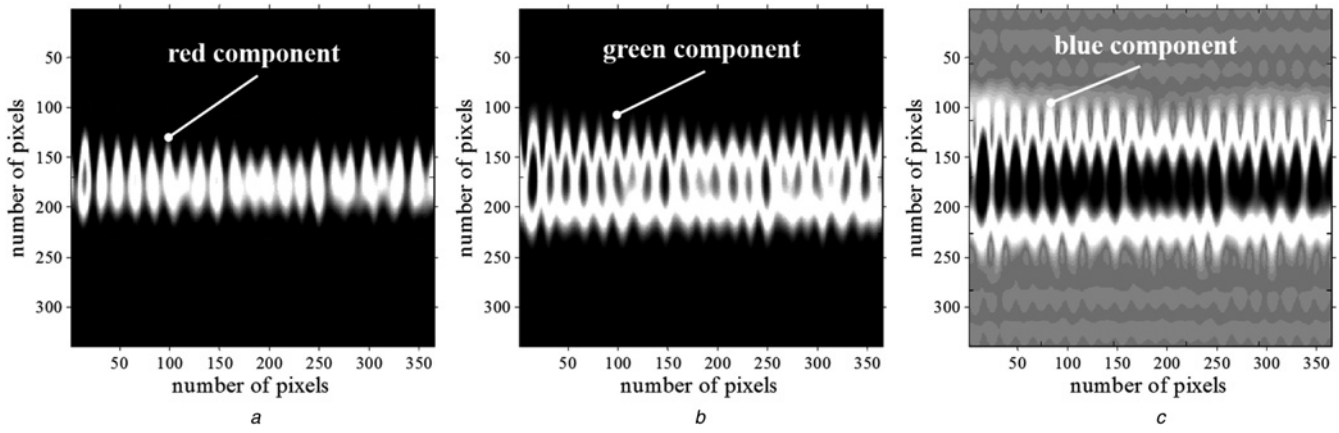


**Fig. 4** *Image components extracted from the RGB image*

*a* Red component
*b* Green component
*c* Blue component


*IET Radar Sonar Navig.*, 2015, Vol. 9, Iss. 7, pp. 783–789

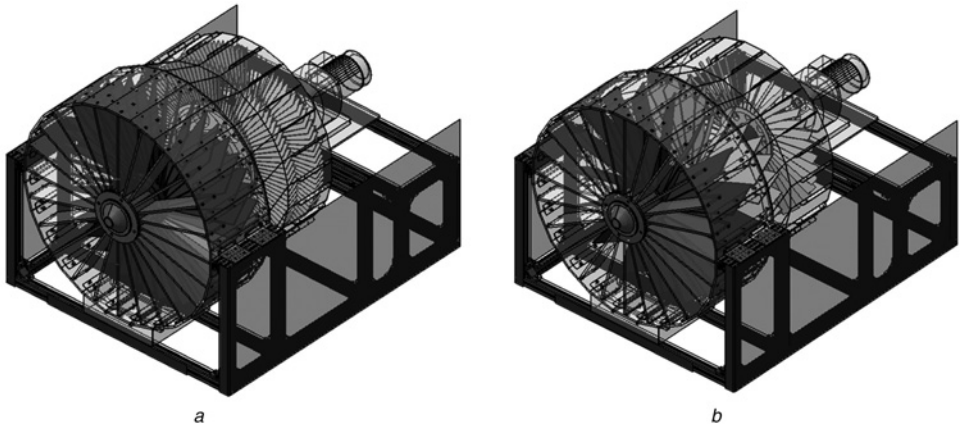

**Fig. 5** *Complete CAD of the fabricated jet engine models*

*a* Type A
*b* Type B

frequency offset is removed from the SPWVD result using the frequency shifting, the BL can be calculated without considering the cavity effect as follows

$$\mathrm{BL} = \frac{\lambda f_{\mathrm{d,\,max}}}{2\omega \sin\alpha} = \frac{\lambda}{2\omega \sin\alpha} \cdot \left[ \left( \frac{\mathrm{VPN} - 1}{2} - \mathrm{MP} \right) \cdot \frac{\mathrm{FR}}{\mathrm{VPN}} \right] \quad (3)$$

where MP is the minimum index of the vertical pixel that corresponds to the peak of the upper contour, VPN is the number of pixels in the vertical axis and FR is the full range of the frequency axis in the JTF representation. Following this, the BL can be obtained using a relative rate between the value of the JTF representation and the number of the pixels in the image domain. For the example case exhibited in Fig. 3, FR can be found as 599 from the JTF representation in Fig. 1*d*, and VPN is obtained as 339 as denoted in Fig. 3*c*. Among the vertical pixel indices of the peaks detected from the upper contour, the minimum index can be found as 95, which is designated as MP. Consequently, the BL can be calculated as 0.394 using (3).

The proposed image processing method makes the overall procedures for jet engine feature extraction more accurate and efficient than the original approach in the sense that the jet engine information is obtained from the JTF representation of JEM signals not manually but automatically.

**Table 1** Structural information on the experimental jet engine models and measurement parameters

| Parameter | | Value | | |
|---|---|---|---|---|
| rotor stage number | | 1 | 2 | 3 |
| type A | BN | 42 | 73 | 97 |
| | BL | 0.377 m | 0.275 m | 0.275 m |
| | rotation speed | | 60.1 RPM | |
| type B | BN | 17 | 29 | 41 |
| | BL | 0.385 m | 0.325 m | 0.300 m |
| | rotation speed | | 180.7 RPM | |
| radar carrier frequency | | | 10 GHz | |
| radar observation (incident) angle | | | 50° | |
| PRF | | | 1.8 kHz | |

## 3 Verification with measured Jem signals

In this section, measured JEM signals are examined to verify the proposed method for automatic feature extraction. In [22], experimental jet engine models were fabricated and measurement was conducted using the instrumentation radar system for various aspect angles and engine rotation speeds. Their complete CAD models are shown in Fig. 5. The structural information on the jet engine models and measurement parameters are given in Table 1. For a fixed radar aspect angle of 50°, we selected two signals from different engine types with different rotating speeds.

Fig. 6 shows the JTF representation of the JEM signal from a type A engine with a rotation speed of 60.1 RPM. As described previously, SPWVD was applied to IMF 1 combined with the last IMF (IMF 13 in this case) and can exhibit a periodic and regular

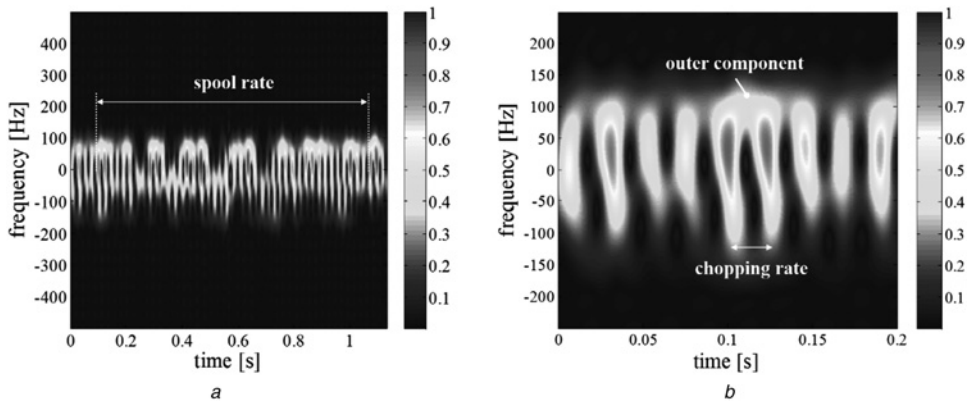


**Fig. 6** *JTF representation of the JEM signal from a type A engine rotating at the rage of 60.1 RPM*

*a* SPWVD result
*b* Expanded SPWVD result related to a

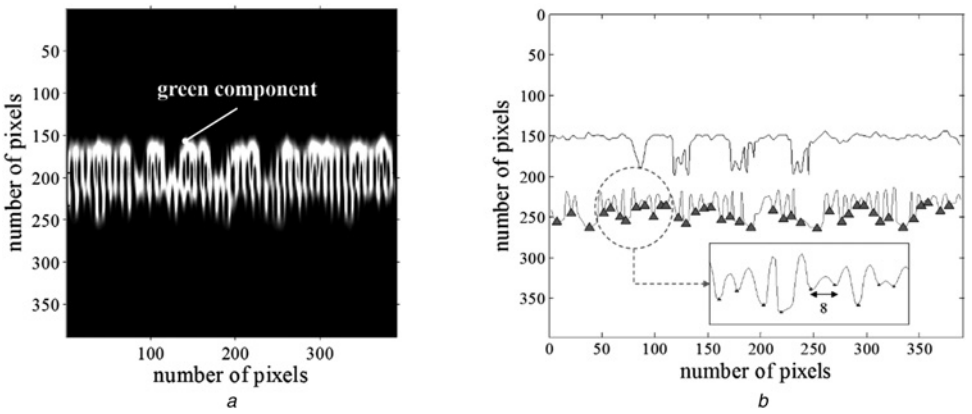


**Fig. 7** *Result of image processing from JTF representation of the JEM signal from a type A engine*

*a* Green component extracted from the RGB image
*b* Peaks detected from the selected contour

waveform in the JTF domain. Note that the length of the smoothing functions for SPWVD were chosen as 22 ms for sufficient time-frequency resolution. The spool rate, the full rotation period, can be found using the periodically repeating partial group as marked in the SPWVD result of Fig. 6*a*. The chopping rate, the period when a blade moves to its adjacent position, can also be estimated from the expanded SPWVD result in Fig. 6*b*. Furthermore, the maximum Doppler frequency can be extracted from the outer components of the Doppler span as marked in Fig. 6*b*. To obtain the jet engine features automatically rather than manually, we apply the proposed image processing method to the JTF representation in Fig. 7.

Fig. 7 shows the result of image processing. Fig. 7*a* shows the green component of the RGB image converted from the JTF representation of a type A signal. Each white pixel corresponds to the green component of the RGB image at a specific spatial location. Fig. 7*b* presents two contours extracted from the green component and the peaks of the lower contour, which was selected on the basis of variance. From Fig. 7*b*, HPN, FP, MP and VPN can be obtained as 390, 8, 144 and 392, respectively. From the JTF representation in Fig. 6*a*, TR and FR can be estimated as 1.1319 and 999. $f_R$ can be found as 1.0345 Hz, using the time interval between auto-correlation function peaks. Using (1) and (3), the important information on the type A engine, such as the BN and the BL, can be obtained as summarised in Table 2. From Table 2, we can observe that not only the exact number of blades but also the BL can be automatically estimated with an error of 4.8%, which originates from the remaining cavity effect and the smoothing function of SPWVD. Note that the JEM chopping harmonics are chiefly generated by the first rotor stage of the engine because the rotation of this stage primarily contributes to the JEM effect.

**Table 2** Estimated information on the examined jet engine models

| Type | BN | | | BL | | |
|---|---|---|---|---|---|---|
| | Real | Estimated | Error | Real | Estimated | Error, % |
| A | 42 | 42 | 0 | 0.377 m | 0.395 m | 4.8 |
| B | 17 | 17 | 0 | 0.385 m | 0.402 m | 4.4 |

Fig. 8 shows the JTF representation of the signal from a type B engine when it rotates at a rate of 180.7 RPM. For this type, the length of the smoothing functions for SPWVD were given as 7.3 ms. On account of the increased rotation speed, the related parameters, such as the length of the smoothing functions are correspondingly reduced as described chapter 2.1. With the refined SPWVD result, we can obtain the information on the jet engine model, such as the spool rate, the chopping rate and the outer component related to the BL. Fig. 9*a* shows the green component extracted from the JTF representation depicted in Figs. 8 and 9*b* presents the peaks detected from the selected contour of the green component. In this case, the vertical pixel distance between the upper and lower contours increases in relation to that of the type A case shown in Fig. 7*b*. This is because the rotation speed is faster than that of type A.

Information on a type B engine is summarised in Table 2 and shows quite a good match with the real parameters. Application results with the measured JEM signals confirm that the proposed

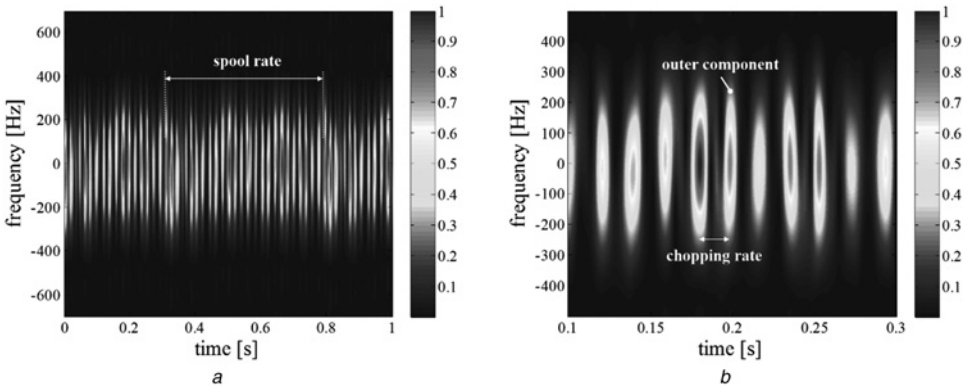


**Fig. 8** *JTF representation of the JEM signal from a type B engine rotating at a rate of 180.7 RPM*

*a* SPWVD result
*b* Expanded SPWVD result related to *a*


*IET Radar Sonar Navig.*, 2015, Vol. 9, Iss. 7, pp. 783–789

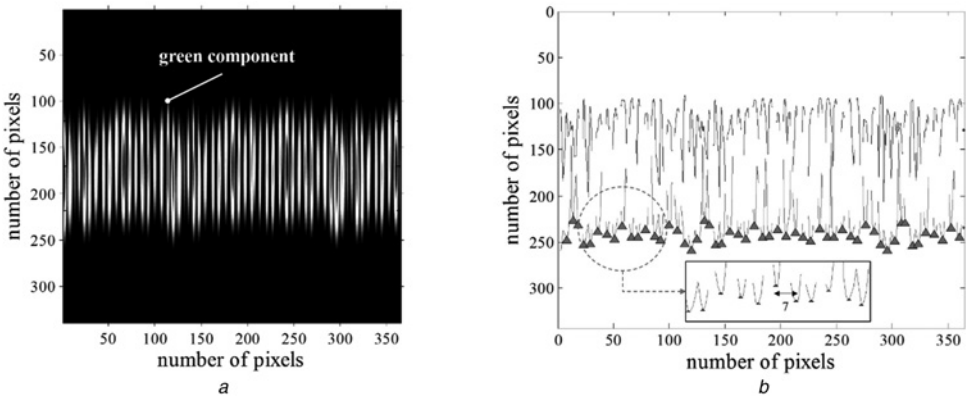


**Fig. 9** *Result of image processing from JTF representation of the JEM signal from a type B engine*

*a* Green component extracted from the RGB image
*b* Peaks detected from the selected contour

method for automatic extraction is effective in accurately and efficiently estimating jet engine features.

## 4 Conclusion

This paper presented automatic extraction of jet engine features using measured signals. To concentrate on the first chopping harmonic, we used the EMD combined with the adaptive LPF. The SPWVD result of the sum of IMF 1 and the last IMF yielded a refined JTF representation. After converting the SPWVD result into an image with RGB colours, the green component was extracted as a representative of the JEM component. Then, peak detection was performed for the fast-varying contour of the green component and enabled us to automatically obtain the information on the jet engine. Consequently, the proposed method for automatic feature extraction significantly improved the accuracy of the JEM analysis and is expected to be efficient for real-time NCTR. Future work should focus on application to measured signals for which the first chopping component harmonic becomes relatively small in relation to other spectral components.

## 5 Acknowledgment

This research was supported by Samsung Thales Co., Ltd.

## 6 References

1 Chen, V.C.: 'The micro-Doppler effect in radar' (Artech House, Norwood, MA, 2011)
2 Chen, V.C., Li, F., Ho, S.S., Wechsler, H.: 'Micro Doppler effect in radar: Phenomenon, model and simulation study', *IEEE Trans. Aerosp. Electron. Syst.*, 2006, **42**, (1), pp. 2–21
3 Chen, V.C., Miceli, W., Himed, B.: 'Micro-Doppler analysis in ISAR – review and perspectives'. IEEE Int. Radar Conf. Surveillance for a Safer World, Bordeaux, France, October 2009, pp. 1–6
4 Zhang, Q., Yeo, T.S., Tan, H.S., Luo, Y.: 'Imaging of a moving target with rotating parts based on the Hough transform', *IEEE Trans. Geosci. Remote Sens.*, 2008, **46**, (1), pp. 291–299
5 Tait, P.: 'Introduction to radar target recognition', Sonar and Navigation Series 18 (IET Radar, 2005)
6 Lim, H.: 'Scattering and feature analysis of jet engine modulation effect of aircraft engine models for non-cooperative target recognition'. Ph.D. thesis, Korean Advanced Institute of Science and Technology (KAIST), 2011
7 Cuomo, S., Pellegrini, P.F., Piazza, E.: 'Model validation for 'jet engine modulation' phenomenon', *Electron. Lett.*, 1994, **30**, pp. 2073–2074
8 Ai, X., Yan, H., Zhao, F., Yang, J., Li, Y., Xiao, S.: 'Imaging of spinning targets via narrow-band T/R-R bistatic radars', *IEEE Geosci. Remote Sens. Lett.*, 2013, **10**, (2), pp. 362–366
9 Ai, X., Li, Y., Wang, X., Xiao, S.: 'Feature extraction of rotational yargets in wideband T/R–R bistatic radar', *IET Radar Sonar Navig.*, 2013, **7**, (4), pp. 351–360
10 Cai, C., Liu, W., Fu, J.S., Lu, Y.: 'Radar micro-Doppler signature analysis with HHT', *IEEE Trans. Aerosp. Electron. Syst.*, 2010, **46**, (2), pp. 929–938
11 Thayaparan, T., Abrol, S., Riseborough, E., *et al.*: 'Analysis of radar micro-Doppler signatures from experimental helicopter and human data', *IET Radar Sonar Navig.*, 2007, **1**, pp. 289–299
12 Setlur, P., Ahmadn, F., Amin, M.: 'Helicopter radar return analysis: Estimation and blade number selection', *Signal Process.*, 2011, **91**, pp. 1409–1424
13 Pan, X., Wang, W., Liu, J., *et al.*: 'Features extraction of rotationally symmetric ballistic targets based on micro-doppler', *Prog. Electromagn. Res.*, 2013, **137**, pp. 727–740
14 Lim, H., Park, J.H., Yoo, J.H., *et al.*: 'Joint time-frequency analysis of radar micro-Doppler signatures from aircraft engine models', *J. Electromagn. Waves Appl.*, 2011, **25**, pp. 1069–1080
15 Park, J.H., Lim, H., Myung, N.H.: 'Modified Hilbert-Huang transform and its application to measured micro Doppler signatures from realistic jet engine models', *Prog. Electromagn. Res.*, 2012, **126**, pp. 255–268
16 Park, J.H., Myung, N.H.: 'Effective reconstruction of the rotation-induced micro-Doppler from a noise-corrupted signature', *Prog. Electromagn. Res.*, 2013, **138**, pp. 499–518
17 Bai, X., Xing, M., Zhou, F., Lu, G., Bao, Z.: 'Imaging of micromotion targets with rotating parts based on empirical mode decomposition', *IEEE Trans. Geosci. Remote Sens.*, 2008, **46**, (11), pp. 3514–3523
18 Yan, R., Gao, R.X.: 'A tour of the Hilbert-Huang transform: An empirical tool for signal analysis', *IEEE Instrum. Meas. Mag.*, 2007, **10**, (5), pp. 40–45
19 Mostafanezhad, I., Boric-Lubecke, O., Lubecke, V., Mandic, D.: 'Application of empirical mode decomposition in removing fidgeting interference in Doppler radar life signs monitoring devices'. IEEE Engineering in Medicine and Biology, Minneapolis, USA, September 2009, pp. 340–343
20 Sparr, T., Krane, B.: 'Micro-Doppler analysis of vibrating targets in SAR', *IEE Proc. Radar Sonar Navig.*, 2003, **150**, pp. 277–283
21 Pouliguen, P., Lucas, L., Muller, F., Quete, S., Terret, C.: 'Calculation and analysis of electromagnetic scattering by helicopter rotating blades', *IEEE Trans. Antennas Propag.*, 2002, **50**, pp. 1396–1408
22 Lim, H., Yoo, J.H., Kim, C.H., Kwon, K.I., Myung, N.H.: 'Radar cross section measurement of a realistic jet engine structure with rotating parts', *J. Electromagn. Waves Appl.*, 2011, **25**, pp. 999–1008